

Dependence of electronic and optical properties on a high-frequency field for carbon nanotubes

Wenhu Liao¹, Guanghui Zhou^{1,3,*} and Kai-He Ding²

¹*Department of Physics and Key Laboratory of Educational Ministry for Low-Dimensional Quantum Structures and Manipulation, Hunan Normal University, Changsha 410081, China[†]*

²*Department of Physics and Electronic Science, Changsha University of Science and Technology, Changsha 410076, China and*

³*International Center for Materials Physics, Chinese Academy of Sciences, Shenyang 110015, China*

(Dated: October 30, 2018)

We study theoretically the electronic structure, transport and optical properties for a zigzag single-wall carbon nanotube connected to two normal conductor leads under the irradiation of an external electromagnetic field at low temperatures, with particular emphasis on the features of high-frequency response. Using the standard nonequilibrium Green's function techniques, we examine the time-averaged density of states, the conductivity, the dielectric function and the electron energy loss spectra for the system with photon polarization parallel with the tunneling current direction, respectively. Through some numerical examples, it is shown that the density of states is strongly dependent on the incident electron energy, the strength and frequency of the applied field. For higher electron energies in comparison with lead-nanotube coupling energy, the system conductance decreases with increasing the field strength and increases with increasing the field frequency respectively, and shows some oscillation structures. Moreover, the optical functions for the system have also a rich structure with the variation of field frequency. It may demonstrate that this transport dependence on the external field parameters can be used to give the energy spectra information of carbon nanotubes and to detect the high-frequency microwave irradiation.

PACS numbers: 73.23.-b, 73.63.Fg

I. INTRODUCTION

Nanoelectronics, or molecular electronics, have been proposed as the alternative to silicon in future technical applications¹ and have attracted much interest recently. Especially, carbon based nanostructures, such as fullerene, graphene and nanotubes, are the most interesting structures because of their excellent physical and chemical properties. Carbon nanotubes (CNTs) can exhibit metallic or semiconducting behavior with different diameter and chirality, and therefore they will be promising candidates for the new carbon-nanotube-based electronic devices, such as nanosensors,² electric batteries,³ field-effect transistors,^{4,5} Coulomb blockade devices,^{6,7} and field-emission displays.⁸

The quantum transport properties of CNT systems have been investigated experimentally by many authors.^{9–11} The coherent quantum wire behaviors of an individual single-walled carbon nanotube (SWCNT)⁹ between two contacts and the conductance quantization of multi-walled CNTs¹⁰ have been observed, respectively. Moreover, Onac *et al.*¹¹ have used an on-chip to detect the high-frequency noise signals generated by quantum dot formed in a SWCNT with photon-assisted tunneling. This result so far indicates no intrinsic frequency limitation due to the CNTs themselves. Using the long-wavelength approximation, Mele *et al.*¹² have studied the coherent one-photon and two-photon electronic excitations for graphene sheets and SWCNTs. The optical dielectric function of a finite SWCNT has also been studied early by gradient approximation¹³ and by first-principle calculations,¹⁴ respectively. Furthermore, the conductances for microwave

field irradiated multiwall CNT¹⁵ and SWCNT¹⁶ connected to two leads have been investigated by photon-assisted transport model, in which the conductance oscillations evolve toward a well-defined step structure and its sensitive dependence on the field intensity have been expected.¹⁶ This study has been extended¹⁷ to optical selection rule for SWCNT very recently. The question thus arises whether SWCNTs could be useful as terahertz (THz) detection, which is more important in the use of quantum control to nanostructures. To the best of our acknowledge, this important case for a driven SWCNT-based system has not been reported previously.

In this paper, we present a theoretical investigation of the electronic structure, transport and optical properties for a metallic zigzag chiral SWCNT under a THz electromagnetic field (EMF) irradiation since metallic CNTs are known to be one of the ideal system exhibiting quantum mechanical nature of the electrical transport.¹⁵ The dependence of time-averaged electron density of states (DOS), conductance, dielectric function (ϵ) and electron energy loss spectrum (EELS) on the irradiation field strength and frequency are demonstrated for the system, respectively. Some different characteristics is obtained and the results are compared with those for the similar physical systems in the previous works.^{9,13–17}

The rest of the paper is organized as follows. The analytical expressions of the time-averaged DOS, the conductance and the optical functions are calculated starting from the system Hamiltonian by NGF approach in Sec. II. Some numerical examples and discussions for the results are demonstrated in Sec. III. Finally, Sec. IV concludes the paper.

II. MODEL AND FORMULISM

The NGF approach has been employed in last decades to study transport problems involving variety of interactions be-

[†]Mailing address

yond the linear response regime.¹⁸ Meir *et al.*¹⁹ have derived a formula for the current through a region of interacting electrons using the nonequilibrium Keldysh formalism. Here we assume that the external high-frequency field only causes a rigid shift in the electron energy spectrum under the widely adopted adiabatic approximation. Therefore, the Hamiltonian for an irradiated SWCNT embedded between two normal conductor leads reads

$$\begin{aligned}
H = & \sum_{q,\alpha \in L/R} \epsilon_{q,\alpha} d_{q,\alpha}^\dagger d_{q,\alpha} + \sum_k \epsilon_k c_k^\dagger c_k \\
& + \sum_{q,\alpha \in L/R,k} (V_{q,\alpha,k} d_{q,\alpha}^\dagger c_k + V_{q,\alpha,k}^* c_k^\dagger d_{q,\alpha}) \\
& + \sum_{k,k'} V_0 \cos(\omega t) c_k^\dagger c_{k'}, \quad (1)
\end{aligned}$$

where the operator $d_{q,\alpha}^\dagger$ ($d_{q,\alpha}$) creates (annihilates) an electron with momentum q in mode α in either left (L) or right (R) lead, and c_k^\dagger (c_k) creates (annihilates) an electron at the state k of the CNT with energy spectrum^{13,20} $\epsilon_k = \pm\gamma[3 + 2 \cos(2k_y b) + 4 \cos(k_x b) \cos(3k_x a)]^{1/2}$, which is similar as that of graphene though the boundary conditions of SWCNT are different from graphene, especially in the circle direction. Where γ is the hopping integral of CNT in the tight-banding approximation, $a \approx 0.71 \text{ \AA}$ is the half length of in-plane lattice constant with $b = \sqrt{3}a$, and k_x and k_y are in-plane wavevectors of Dirac electron. The coupling between the electrode leads and the CNT with strength $V_{q,\alpha,k}$ is represented by the third term in Hamiltonian (1), and the last term describes the electron-photon interaction in the CNT, where V_0 is the interaction strength un-

der dipole approximation and ω the incident field frequency. Moreover, for simplicity, in the above Hamiltonian we have neglected the spin and electron-electron interactions although much attention has been paid to the pseudospin-related effects in graphenes²¹ and SWCNTs.²²

Now we employ the usually defined retarded and correlated Green's Function (GF)^{16,18,19} as $G_k^r(t_2, t_1) = \mp i \theta(\pm t_2 \mp t_1) \langle \{c_k(t_2), c_k^\dagger(t_1)\} \rangle$ and $G_k^<(t_2, t_1) = -i \langle \{c_k(t_1), c_k^\dagger(t_2)\} \rangle$ to the Hamiltonian. When the unperturbed GF $g^r(\epsilon)$ of the nanotube is obtained, one can obtain GFs of $G^r(\epsilon)$ and $G^<(\epsilon)$ from the Dyson equation $G^r(\epsilon) = [(g^r(\epsilon))^{-1} - \Sigma^r(\epsilon)]^{-1}$ and the Keldysh equation $G^<(\epsilon) = G^r(\epsilon) \Sigma^<(\epsilon) G^a(\epsilon)$, respectively. Furthermore, the self-energies are $\Sigma^r(\epsilon) = (-i/2)[\Sigma^L(\epsilon) + \Sigma^R(\epsilon)]$ and $\Sigma^<(\epsilon) = (-i/2)[f_L(\epsilon)\Sigma^L(\epsilon) + f_R(\epsilon)\Sigma^R(\epsilon)]$, where the linewidth function $\Sigma^\alpha(\epsilon) = 2\pi \sum_{q,k} V_{q,\alpha,k}^* V_{q,\alpha,k} \delta(\epsilon - \epsilon_{q,\alpha})$ describes the influence of the leads and $f_\alpha(\epsilon)$ is the Fermi distribution function. In the wide-bandwidth approximation,^{15,16,18,19} $\Sigma^\alpha(\epsilon)$ is taken to be independent of the energy and energy levels.

Furthermore, the GF of a honeycomb lattice (graphene) can be written as

$$g_k^r(\epsilon) = \frac{\epsilon/\gamma}{\epsilon^2 - 3 - 2 \cos(2k_y b) - 4 \cos(k_y b) \cos(3k_x a)}. \quad (2)$$

For a $(n, 0)$ chiral zigzag SWCNT, the periodic boundary conditions^{13,16} requires that the transverse wave vector k_y supplies $k_y b = \pi j/n$ with good quantum numbers for the subbands $j=1 \sim 2n$, and the longitudinal wave vector k_x is confined in the first Brillouin zone $-\pi/(3a) < k_x < \pi/(3a)$. Applying Fourier transform to $g_k^r(\epsilon)$ one obtains the unperturbed GF in the real space

$$g^r(\epsilon, l, m) = \frac{6ab\epsilon}{4\pi^2\gamma} \sum_{j=1}^{2n} \int_{-\pi/(3a)}^{\pi/(3a)} dk_x \frac{e^{-3ik_x la} e^{-i\pi jm/n}}{\epsilon^2 - 3 - 2 \cos(2\pi j/n) - 4 \cos(\pi j/n) \cos(3k_x a)}, \quad (3)$$

where l and m are respectively the length and width index in real space, once the integration over k_x is done in Eq. (3), one can obtain the analytical expression of $G^r(\epsilon)$ from Dyson equation. Therefore, the real part of the zero-bias limit linear conductance¹⁵⁻¹⁷ can be derived as

$$\begin{aligned}
\sigma_1(V_0, \omega) = & \frac{2e^2}{h} \int d\epsilon \sum_\mu J_\mu^2\left(\frac{V_0}{\hbar\omega}\right) \\
& \times \left(-\frac{\partial f(\epsilon)}{\partial \epsilon} \right) \Sigma^L G^r(\epsilon) \Sigma^R G^a(\epsilon), \quad (4)
\end{aligned}$$

where $J_\mu(x)$ is the μ th-order Bessel function of the first kind. The imaginary part of conductance, $\sigma_2(V_0, \omega)$, can be calculated from $\sigma_1(V_0, \omega)$ by Kramers-Kronig transformation^{14,17}

$$\sigma_1(V_0, \omega) = 1 + \frac{4}{\pi} \mathbf{P} \int_0^\infty d\omega' \frac{\omega' \sigma_2(V_0, \omega')}{\omega'^2 - \omega^2}, \quad (5)$$

where \mathbf{P} denotes the principal value of the integral. From the

complex dielectric function $\epsilon(V_0, \omega) = 1 + 4\pi i \sigma(V_0, \omega)/\omega$ with $\sigma(V_0, \omega) = \sigma_1(V_0, \omega) + i\sigma_2(V_0, \omega)$, in principle one can obtain all other linear optical properties such as reflectivity, absorption spectrum and EELS by $-\Im m[\epsilon(V_0, \omega)]^{-1}$ at the long-wavelength limit,^{13,14} where $\Im m$ represents the imaginary part of the quantity. The effective electron DOS will be¹⁶

$$D(\epsilon) = \sum_\mu \left| J_\mu\left(\frac{V_0}{\hbar\omega}\right) \right|^2 D_0(\epsilon - \mu\hbar\omega), \quad (6)$$

In the tight-banding approximation, the DOS of a $(n, 0)$ CNT in the absence of perturbing potential reads²²

$$\begin{aligned}
D_0(\epsilon) = & \frac{2}{3\pi^2} \Im m \sum_{j=1}^{2n} i(\epsilon + i0^+) \times \{8[1 + \cos(2\pi j/n)] \\
& - [(\epsilon + i0^+)^2 - 2 \cos(2\pi j/n) - 3]^2\}^{-1/2}. \quad (7)
\end{aligned}$$

It should be pointed out that Eq. (6) can be interpreted as

following. Photon absorption ($\mu>0$) or emission ($\mu<0$) can be viewed as creating an effective electron DOS at sideband energies $\epsilon_\mu=\mu\hbar\omega$ with a probability $|J_\mu(V_0/\hbar\omega)|^2$. One notes that the multi-photon processes will be suppressed more or less in the cases of $V_0/(\hbar\omega)\gg 1$, and the enough strong EM field ($V_0/(\hbar\omega)\gg 1$ cases) will split sharp singularities in the electron spectrum except for its affection on the electron distribution of the CNT.²³ Therefore, in this work we concentrate on the cases of the relatively high-frequency response under moderate irradiation field strength for the system.

III. RESULTS AND DISCUSSIONS

In the following, we present some numerical examples of the calculated normalized DOS, linear conductance and optical properties for an external field irradiated (12,0) SWCNT. The tight-banding approximation hopping integral $\gamma=2.75$ eV is taken to be the unit of energy, the temperature²⁴ and the effective ‘speed of light’ are $k_B T=0.01$ and $v_F=8.88\times 10^5$ m/s, respectively. In our numerical calculation, the geometry index l and m in Eq. (3) are selected as 12 and 24 for a SWCNT system, that is, the diameter and length of the CNT is about 1 nm and 2.6 nm, respectively. In the wide-band approximation,^{15,16,18,19} we assume that $\Sigma^L=\Sigma^R=\Sigma=0.001\gamma$ as the CNT-lead coupling parameter for simplicity. The above selected parameters for the system are reachable in the present experiments.^{9–11}

Figure 1 shows the calculated time-averaged DOS (in arbitrary units) and linear conductance σ_1 (in units of $\sigma_0=2e^2/h$) as a function of the incident electron energy ϵ (in units of γ) with a fixed field frequency $\nu=\omega/(2\pi)=33.25$ THz for different field strength V_0 . In the absence of irradiation field, as shown by the solid line in Fig. 1(a), the DOS presents a series of original peaks at energies ± 0.40 , ± 0.50 , ± 0.75 and ± 0.95 , respectively. A wide van Hove pseudogap is observed wherever the DOS is not zero. However, when an irradiation field of strength $V_0=1.1$ eV with photon energy $\hbar\nu=0.05\gamma$ is applied, as shown by the dashed line in Fig. 1(a), except for a series of resonance peaks in low energy range of $-0.40\gamma<\epsilon<0.40\gamma$, there are some resonance peaks at ± 0.55 , ± 0.60 , ± 0.65 , ± 0.70 , ± 0.80 , ± 0.85 and $\pm 0.95\gamma$, respectively. These additional peaks are mainly attributed to the processes of 1-photon and 3-photon processes. Moreover, in the case of field strength $V_0=2.20$ eV [see the dotted line in Fig. 1(a)] with the same field frequency, due to the 2-photon, 4-photon and 6-photon processes, the system DOS presents a much richer structure except for a remarkably changed van Hove pseudogap. This result is quantitatively different from that in Ref. 16 (see, e.g., Fig. 2 in Ref. 16) where no quantitative explanation about the electronic structures was given. The sensitive dependence of DOS on the irradiation field strength can be physically interpreted as following. With a certain photon frequency, the variation of the field strength should be followed by different photon sideband processes as can be verified from Eq. (6). Furthermore, the electronic structures of an irradiated (10, 0) zigzag SWCNT (semiconducting type) have also been plotted with the same parameters (not shown here), the

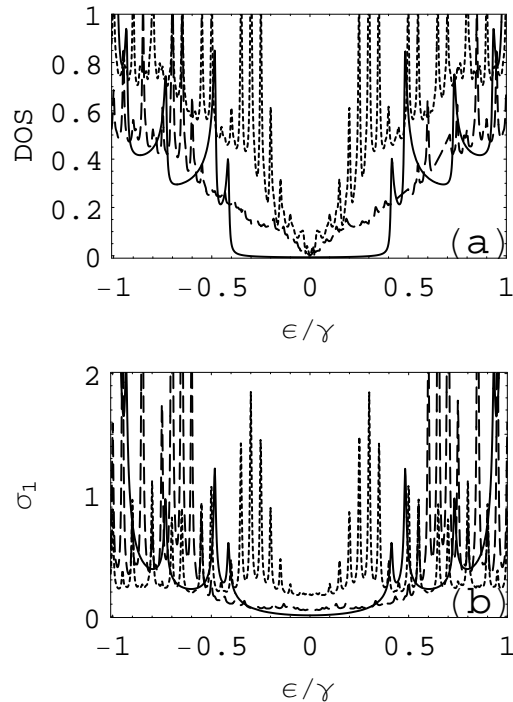


FIG. 1: The dependence of (a) time-averaged DOS and (b) conductance on the incident electron energy ϵ with a field frequency $\nu=33.25$ THz for three different field strengths, where solid line [down-shifted 0.1 for comparison in (a)] for $V_0=0$, dashed line for $V_0=1.1$ eV and dotted line [up-shifted 0.1 for comparison in (b)] for $V_0=2.2$ eV, respectively.

results are similar except for a wider van Hove pseudogap is observed.

The corresponding real part conductance σ_1 to Fig. 1(a) is illustrated in Fig. 1(b). In the absence of external field, as shown by the solid line in Fig. 1(b), σ_1 presents a peak at the four original resonance states and σ_1 is nearly 0 in the pseudogap as expected. Wherever, under the irradiation of a field with strength of $V_0=1.10$ eV, as shown by the dashed line in Fig. 1(b), the system conductance presents a series of additional peaks at ± 0.55 , ± 0.60 , ± 0.65 , ± 0.70 , ± 0.75 and $\pm 0.85\gamma$, respectively. When the field strength increases to 2.20 eV, one can find several additional conductance peaks at ± 0.15 , ± 0.20 , ± 0.25 and $\pm 0.30\gamma$ in the low energy range [as shown by the dotted line in Fig. 1(b)] owing to multi-photon processes, while the conductance peaks in the higher energy range are unchanged.

In what follows, we show the influences of the external field parameters on the electronic structure and transport of the system for a fixed incident electron energy $\epsilon=8\gamma/11$ (2.0 eV). Fig. 2 depicts the time-averaged DOS and σ_1 as a function of the irradiation field strength ($\sim V_0$). In the case of a relative low field frequency $\nu=33.25$ THz, as shown by the solid line in Fig. 2(a), the DOS decreases slowly with an oscillating periodicity about 0.5 eV other than a step at $0.50<V_0<1.0$ eV. When the field frequency increases to $\nu=49.9$ THz (dashed line) and $\nu=66.5$ THz (dotted line) as shown in Fig. 2(a), the oscillating

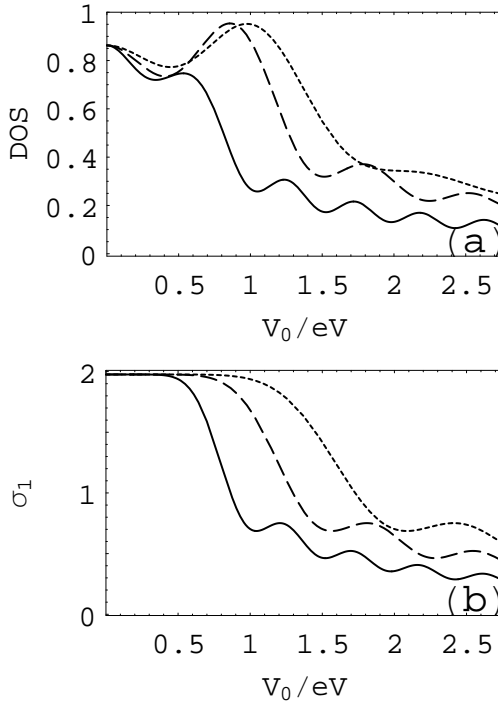


FIG. 2: The dependence of (a) time-averaged DOS and (b) conductance on the field strength with a fixed energy $\epsilon=2.0$ eV for three different field frequencies, where solid line for $\nu=33.25$ THz, dashed line for $\nu=49.9$ THz and dotted line for $\nu=66.5$ THz, respectively.

periodicity seems to become larger except for a peak at 0.9 eV and 1.0 eV, respectively.

Figure 2(b) illustrates the behavior of σ_1 as a function of the field strength for three different field frequencies. In the case of low frequency $\nu=33.25$ THz, as shown in the solid line, σ_1 presents a downgrade step-like structure with oscillating periodicity about 0.5 eV similar to that of the DOS [see Fig. 2(a)]. When the field frequency increases to $\nu=49.9$ THz or $\nu=66.5$ THz, as shown in the dashed line or dotted line of Fig. 2(b), the oscillating periodicity becomes larger. As mentioned above, due to the case of higher frequency for the system we have considered, the results here are quantitatively different from those in Ref. 16 (see, e.g., Figs. 4 and 6 in Ref. 16) where well-defined up-going step structures for the conductance have been predicted only for very low ($\nu < 3.3$ THz) field frequencies with zero incident electrons energy and temperature. It should be pointed out that the results here are qualitatively different those in Ref. 15 (see, e.g., Figs. 2 and 3 in Ref. 15) where a nearly universal down-going normalized resistance with the microwave power and frequency-irrelevant normalized resistance at liquid helium temperature have been observed. Moreover, the electronic structures and conductance of a longer zigzag SWCNT have been plotted (not shown here) with the same all other parameters, the results are qualitatively similar as expected.

Figure 3 demonstrates the calculated time-averaged DOS and conductance σ_1 as a function of the irradiation field frequency ν (in units of THz) with a fixed incident electron en-

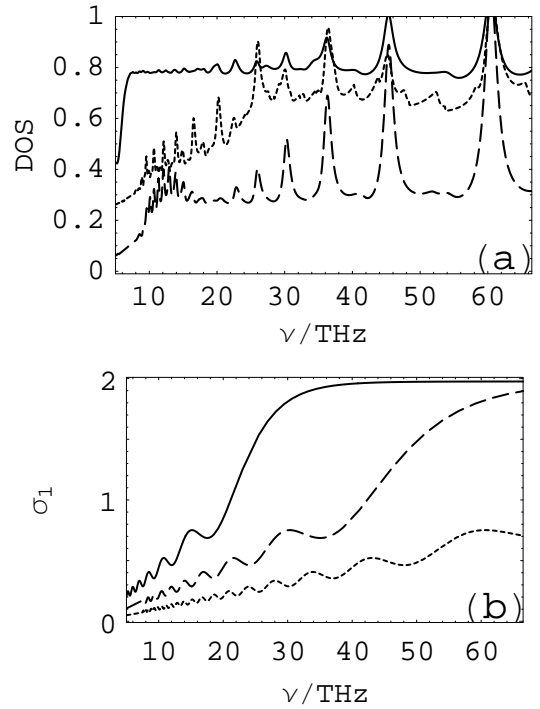


FIG. 3: The dependence of (a) time-averaged DOS and (b) conductance on the field frequency with a fixed incident electrons energy $\epsilon=2.0$ eV for three different field strengths, where solid line for $V_0=0.55$ eV, dashed line for $V_0=1.1$ eV and dotted line [up-shifted 0.2 for comparison in (a)] for $V_0=2.2$ eV, respectively.

ergy $\epsilon=2.0$ eV (same as in Figure 2) for three different field strengths. As shown in Fig. 3(a), one notices that in all case of field strength there is a series of peaks at frequencies $\nu=10, 12, 14, 16.5, 20, 22.5, 26, 30, 36, 45.5$ and 60 THz, respectively. Owing to the difference of the field strengths, these peaks should result from different photons processes as mentioned above and the characteristics will be manifested in the conductance more or less. The behavior of the time-averaged normalized conductance σ_1 versus the field frequency for different strengths is illustrated in Fig. 3(b). In the case of smaller strength $V_0=0.55$ eV (see the solid line), σ_1 presents a rapidly oscillatory up-going structure with the increase of field frequency, and reaching almost $2.0\sigma_0$ as field frequency reaches 36.5 THz. However, when V_0 increases to 1.10 eV, as shown the dashed line in Fig. 3(b), σ_1 up-goes slowly, only two obvious upgrade step-like structures at 20 and 30 THz, respectively. Furthermore, even a much more slowly oscillatory structure is shown by the dotted line in Fig. 3(b) for the case of larger $V_0=2.20$ eV. It should point out that the series of resonance peaks are due to multi-photon processes. The above results are quantitatively different from those in Ref. 16 (see, e.g., Fig. 5 in Ref. 16) where a nearly independence of field frequency in the range of $0 < \nu < 0.005\gamma$ and a higher frequency $0.005\gamma < \nu < 0.05\gamma$ oscillatory response of the conductance have been predicted.

Next, we present numerically the dielectric function $\epsilon(\nu)$ and EELS versus the irradiation field frequency with a fixed

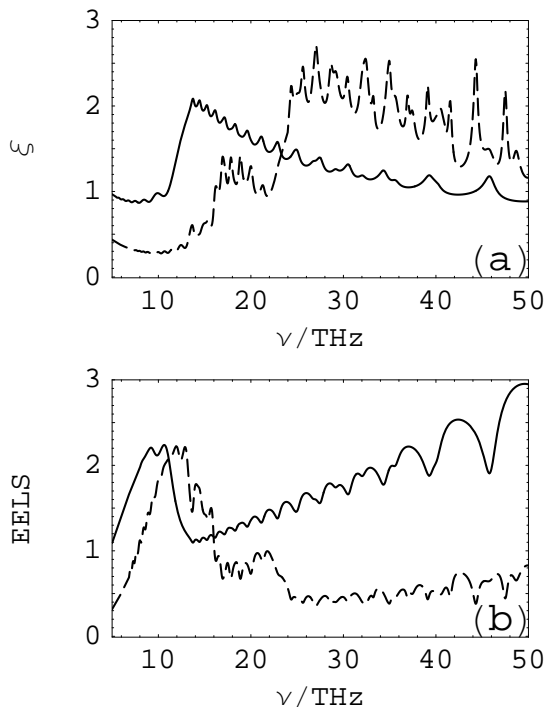


FIG. 4: The dependence of (a) dielectric function $\varepsilon(\nu)$ and (b) electron energy loss spectra (EELS) on the field frequency with a fixed energy $\epsilon=2.75$ meV for two different field strengths, where solid line [up-shifted 0.5 for comparison in (a) and (b)] for $V_0=1.1$ eV and dashed line for $V_0=2.2$ eV, respectively.

incident electron energy (selected as 2.75 meV for comparison with the results in Refs. 14-17) for two different field strengths, and further discuss the basic optical properties¹³⁻¹⁷ of the system. As shown in Fig. 4(a), $\varepsilon(\nu)$ in dashed line, one notices a broad optical absorption frequency strip at the height of 1.0 and 2.0 in the ranges of $16.5 < \nu < 23.5$ THz and $24 < \nu < 30$ THz respectively, with down-going oscillation structures in the range of $30 < \nu < 50$ THz for the case of $V_0=2.2$ eV. Whenever, a peak of near 2.0 height in the vicinity of 13.5 THz with down-going oscillation structures in the higher frequency range for $V_0=1.1$ eV (see the solid line). The characteristics of the $\varepsilon(\nu)$ are different from the results in Refs. 13, 14 and 17 since different parameters we have chosen, although the principal features of Fig. 8 in Ref. 14 have been revealed. Corresponding to the $\varepsilon(\nu)$ as show in Fig. 4(a), the EELS is illustrated in Fig. 4(b). For the case of $V_0=2.2$ eV EELS presents a richer structure as expected since it is related to $\varepsilon(\nu)$ by $-\Im m[\varepsilon(\nu)]^{-1}$. Except for the two broad peaks in the neighbor of 10 and 12 THz for $V_0=1.1$ and 2.2 eV, one notes a optical absorption strip at the height of 1.5 and 0.8 in the ranges of $13.5 < \nu < 16$ THz and $17 < \nu < 23$ THz respectively, with os-

cillation structures around 0.5 in the range of $24 < \nu < 50$ THz for the case of $V_0=2.2$ eV [see the dashed line in Fig. 4(b)]. Since different nanotubes always have a dominating plasmon mode¹³ at ~ 6 eV, therefore, all the above features should rely on multi-photon processes. In short, all the electron DOS, conductance, dielectric function and EELS of CNTs system are sensitive to the strength and the frequency of the external field, which may be applied to the detection of the external THz field and the energy spectra information of carbon nanotubes.

IV. CONCLUSION

In summary, using the NGF method, we have investigated theoretically the electronic structure, transport and optical properties of a metallic-typed zigzag single-wall carbon nanotube connected with two normal leads under the irradiation of an external high-frequency (THz) electromagnetic field at low temperatures. Using the standard nonequilibrium Green's function techniques, we examine the time-averaged density of states, conductance, dielectric function and electron energy loss spectrum for the system with photon polarization parallel with the tunneling current direction, respectively. It is demonstrated that, by analyzing some numerical examples, the density of states shows a strong dependance on the incident electron energy and external field parameters. For high irradiation energies in comparison with CNT-lead coupling, the system conductance decreases with the field strength while increases with the field frequency followed by some oscillation structures. For the lower incident electron energy, the dielectric function and electron energy loss spectrum are consistent with the results in Refs. 13, 14 and 17 due to multi-photon processes. In all cases the system transport and optical properties are sensitive to the parameters of the external field, which may be utilized to the detection of high-frequency irradiation and the energy spectra information of carbon nanotubes. However, the experimental observation for these effects and further theoretical investigations on the system with impurity, spin or electron-electron interactions and the armchair chiral carbon nanotubes are worthy to be carried out.

Acknowledgments

This work was supported by National Natural Science Foundation of China (Grant No. 10574042), Specialized Research Fund for the Doctoral Program of Higher Education of China (Grant No. 20060542002) and Hunan Provincial Natural Science Foundation of China (Grant No. 06JJ2097).

* Electronic address: ghzhou@hunnu.edu.cn

¹ N. J. Tao, Nature Nanotechnology **1**, 173 (2006); P. Avouris, Z. Chen, and V. Perebeinos, Nature Nanotechnology **2**, 605 (2007).

² Y. Chi, Q. Wei, H. Park, and C. M. Lieber, Science **293**, 1289 (2001).

³ Stankovich Sasha, A. Dikin Dmitriy, H. B. Dommett Geoffrey,

- M. Kohlhaas Kevin, J. Zimney Eric, A. Stach Eric, D. Piner Richard, T. Nguyen SonBinh, and S. Ruoff Rodney, *Nature* **442**, 282 (2006).
- ⁴ S. I. Tans, A. Verschueren, and C. Dekker, *Nature* **393**, 49 (1998).
- ⁵ R. Martel, T. Schmidt, H. R. Shea, T. Hertel, and Ph Avouris, *Appl. Phys. Lett.* **73**, 2447 (1998).
- ⁶ L. Chico, V. H. Crespi, L. X. Benedict, S. G. Louie, and M. L. Cohen, *Phys. Rev. Lett.* **76**, 971 (1996).
- ⁷ L. Chico, M. P. Sancho Lopez, and M. C. Munoz, *Phys. Rev. Lett.* **81**, 1278 (1998).
- ⁸ W. B. Choi, D. S. Chung, J. H. Kang, H. Y. Kim, Y. W. Jin, I. T. Han, Y. H. Lee, J. E. Jung, N. S. Lee, G. S. Park, and J. M. Kim, *Appl. Phys. Lett.* **75**, 3129 (1999).
- ⁹ S. J. Tans, Michel H. Devoret, H. J. Dai, Andreas Thess, Richard E. Smalley, L. J. Geerligs, and Cees Dekker, *Nature* **386**, 474 (1997).
- ¹⁰ S. Frank, P. Poncharal, Z. L. Wang, and W. A. de Heer, *Science* **280**, 1744 (1998).
- ¹¹ E. Onac, F. Balestro, B. Trauzettel, C. F. J. Lodewijk, and L. P. Kouwenhoven, *Phys. Rev. Lett.* **96**, 026803 (2006).
- ¹² E. J. Mele, P. Král, and D. Tománek, *Phys. Rev. B* **61**, 7669 (2000).
- ¹³ M. F. Lin and Kenneth W.-K. Shung, *Phys. Rev. B* **50**, 17744 (1994).
- ¹⁴ M. Machón, S. Reich, and C. Thomsen, D. Sánchez-Portal, and P. Ordejón, *Phys. Rev. B* **66**, 155410 (2002); G. Y. Guo, K. C. Chu, Ding-sheng Wang, and Chun-gang Duan, *Phys. Rev. B* **69**, 205416 (2004).
- ¹⁵ Jinhee Kim, Hye-Mi So, Nam Kim, Ju-Jin Kim, and Kicheon Kang, *Phys. Rev. B* **70**, 153402 (2004).
- ¹⁶ P. A. Orellana and M. Pacheco, *Phys. Rev. B* **75**, 115427 (2007).
- ¹⁷ Has Hsu and L. E. Reichl, *Phys. Rev. B* **76**, 045418 (2007).
- ¹⁸ G. Platero and R. Aguado, *Appl. Phys. Lett.* **70**, 3546 (1997); R. Aguado and G. Platero, *Phys. Rev. Lett.* **81**, 4971 (1998); Guanghui Zhou and Wenhui Liao, *J. Phys.: Cond. Mat.* **18**, 9161 (2006).
- ¹⁹ Y. Meir and N. S. Wingreen, *Phys. Rev. Lett.* **68**, 2512 (1992); A. P. Jauho, N. S. Wingreen, and Y. Meir, *Phys. Rev. B* **50**, 5528 (1994).
- ²⁰ R. Saito, M. Fujita, G. Dresselhaus, and M. S. Dresselhaus, *Phys. Rev. B* **46**, 1804 (1994).
- ²¹ M. I. Katsnelson, *Eur. Phys. J. B* **51**, 157 (2006); E. V. Gorbar, V. P. Gusynin, and I. A. Shoykovy, *Phys. Rev. B* **66**, 045108 (2002).
- ²² I. Weymann, J. Barnas, and S. Krompiewski, *Phys. Rev. B* **76**, 155408 (2007); J. Tworzydło, B. Trauzettel, M. Titov, A. Rycerz, and C. W. J. Beenakker, *Phys. Rev. Lett.* **96**, 246802 (2006).
- ²³ S. E. Shafranuk, *Phys. Rev. B* **76**, 085317 (2007); C. Zhang, L. Chen and Z. S. Ma, cond-mat/0709.3700v2.